Scientia Iranica A (2015) 22(5), 1779–1787

Sharif University of Technology
Scientia Iranica
Transactions A: Civil Engineering
www.scientiairanica.com

Research Note

Numerical simulation of flow over labyrinth spillways

Y. Sangsefidi[a], M. Mehraein[b,*] and M. Ghodsian[c]

a. *Faculty of Civil and Environmental Engineering, Tarbiat Modares University, Tehran, Iran.*
b. *Faculty of Engineering, Kharazmi University, Tehran, Iran.*
c. *Water Engineering Research Institute, Faculty of Civil and Environmental Engineering, Tarbiat Modares University, Tehran, Iran.*

Received 30 May 2014; received in revised form 25 February 2015; accepted 11 May 2015

KEYWORDS
Discharge;
Hydraulic performance;
Labyrinth spillway;
Local submergence;
Numerical simulation.

Abstract. Spillways play an important role in the safety of dams. To ensure the safety of dams, spillways should be designed considering floods with long return periods. To increase the discharge capacity of a spillway, a designer can increase the crest length using the labyrinth spillway. For high head conditions, the local submergence may decrease the efficiency of a labyrinth spillway. In this study, the hydraulic characteristics of linear and arced labyrinth spillways are compared, and the effect of the downstream bed level on the discharge coefficient of labyrinth spillways is studied numerically. The numerical simulations are done using Flow-3D software. RNG $k-\varepsilon$ model is used for turbulence simulations and the free-surface profiles are calculated by VOF method. Experimental data of pervious researchers are used for validation of the proposed numerical model. The results show that in the high head conditions, lowering the downstream bed level of a labyrinth spillway increases its efficiency, especially in the case of an arced labyrinth spillway.

1. Introduction

Spillways possess an essential role in the safety of dams and should spill floods with high return periods. Designers of spillways can increase their width to increase the discharge capacity. However, this approach is usually limited to some topography and economic constraints. In such cases, labyrinth spillways are another alternative. Labyrinth spillways can be categorized as linear spillways folded in the plan-view. These spillways provide an increase in the crest length for a given channel width, which causes an increase in the flow capacity for the same head.

One of the first experimental studies on the hydraulic of labyrinth spillways is carried out by Hay and Taylor [1]. They introduced a method for the discharge calculation and the design of triangular and trapezoidal linear labyrinth spillways. Darvas [2] reported laboratory results on trapezoidal linear labyrinth spillway models, which are in close agreement with Hay and Taylor's results. Labyrinth spillways are also studied by research institutions like Utah Water Research Laboratory (UWRL), University of Georgia, and United States Bureau of Reclamation (USBR). Lux and Hinchliff [3], Megalhaes and Lorena [4], Tullis et al. [5], and Khode et al. [6] introduced practical methods for designing linear trapezoidal labyrinth spillways. Falvey [7] summarized a comprehensive review of the previous researches on the labyrinth spillway. Tullis et al. [8] obtained the head-discharge relationships for submerged linear labyrinth spillways. Ghodsian [9] used a dimensional analysis and proposed an equation to estimate the discharge of linear triangular labyrinth spillways. Carollo et al. [10] modified the proposed equation by Ghodsian [9].

*. *Corresponding author. Tel./Fax: +98 21 88830891*
E-mail addresses: yousef.sangsefidi@modares.ac.ir (Y. Sangsefidi); Mojtaba.mehraein@gmail.com (M. Mehraein); Ghods@modares.ac.ir (M. Ghodsian)

More recently, Crookston and Tullis [11,12] studied the hydraulic performance of a trapezoidal arced labyrinth spillway in reservoirs. They reported that the arced labyrinth spillways have higher discharge efficiency (~5 -11% higher than an in-channel labyrinth spillway orientation). Kumar et al. [13,14] showed that the discharge coefficient of an arced spillway located in a channel is smaller than that of a linear spillway. They also reported that by increasing the spillway arc angle (Θ), the discharge coefficient of an arced spillway increases when $\Theta < 90°$. The opposite behavior was observed for $\Theta > 90°$. Christensen [15] indicated that if the number of cycles of an arced labyrinth weir is equal or greater than 5, the discharge coefficient of the weir is independent of the number of cycles.

According to the best knowledge of the authors, most of the previous researches were conducted to study the hydraulic characteristic of a linear labyrinth spillway. Traditionally, labyrinth spillway cycles follow a linear configuration (e.g., Ute Dam in USA); however, arced labyrinth spillways have also been constructed (e.g., Avon Dam in Australia). In this paper, the hydraulic characteristics of labyrinth spillways are numerically studied using Flow-3D software. The hydraulic performance of the arced labyrinth spillway is compared with the in-channel labyrinth configuration, including the effects of approach flow conditions, nappe interference, and local submergence. This paper also studies the effects of the downstream bed level on the discharge coefficient of the labyrinth spillways.

2. Study methods

2.1. Governing equations and computational scheme

Flow-3D solves the modified form of the Reynolds Average Navier-Stokes (RANS) equations. The governing equations are [16]:

$$\frac{\partial}{\partial x}(uA_x)+\frac{\partial}{\partial y}(vA_y)+\frac{\partial}{\partial z}(wA_z)=0, \tag{1}$$

$$\frac{\partial u_i}{\partial t}+\frac{1}{V_F}\left(U_jA_j\frac{\partial u_i}{\partial x_j}\right)=\frac{1}{\rho}\frac{\partial P'}{\partial x_j}+g_i+f_i, \tag{2}$$

where V_F is the fractional volume open to the flow; u, v, and w are the velocities in the x, y, and z directions, respectively; A_x , A_y, and A_z are fractional areas open to the flow in the subscript directions; subscripts i and j represent the flow directions; ρ is the fluid density; t is the time; P' is the pressure; U_j and A_j are the velocity and the face area of the cell in j direction; g_i is the gravitational force in i direction; and f_i represents the Reynolds stresses to close the turbulence model. For the cells full of fluids, V_F and A_j are equal to 1, and the equations are reduced to the incompressible RANS equations.

2.2. Turbulence models

Recently the Renormalization-Group (RNG) is used in turbulence models. These methods use some statistical methods to derive the averaged equations of the turbulence quantities such as dissipation rate and turbulent kinetic energy. The equations of the RNG model are similar to those of the $k-\varepsilon$ model. However, the empirical constants of the RNG model are derived explicitly. The transport equation can be expressed as [16]:

$$\frac{\partial k_T}{\partial t}+\frac{1}{V_F}\left(uA_x\frac{\partial k_T}{\partial x}+vA_y\frac{\partial k_T}{\partial y}+wA_z\frac{\partial k_T}{\partial z}\right)=P_T+G_T+\mathrm{Diff}_T-\varepsilon_T, \tag{3}$$

where k_T is the turbulent kinetic energy, and P_T is the production of turbulent kinetic energy, which can be determined as:

$$\begin{aligned}P_T=&\mathrm{CSPRO}\left(\frac{\mu}{\rho V_F}\right)\left(2A_x\left(\frac{\partial u}{\partial x}\right)^2+2A_y\left(\frac{\partial v}{\partial y}\right)^2\right.\\&+2A_z\left(\frac{\partial w}{\partial z}\right)^2+\left(\frac{\partial v}{\partial x}+\frac{\partial u}{\partial y}\right)\\&\left(A_x\frac{\partial v}{\partial x}+A_y\frac{\partial u}{\partial y}\right)+\left(\frac{\partial u}{\partial z}+\frac{\partial w}{\partial x}\right)\left(A_z\frac{\partial u}{\partial z}\right.\\&\left.\left.+A_x\frac{\partial w}{\partial x}\right)+\left(\frac{\partial v}{\partial z}+\frac{\partial w}{\partial y}\right)\left(A_z\frac{\partial v}{\partial z}+A_y\frac{\partial w}{\partial y}\right)\right),\end{aligned} \tag{4}$$

where μ is the dynamic viscosity, and CSPRO is a turbulence parameter with a default value equal to 1. In Eq. (3), the value of the buoyancy production term, G_T, can be determined as:

$$G_T=-\mathrm{CRHO}\left(\frac{\mu}{\rho^3}\right)\left(\frac{\partial\rho}{\partial x}\frac{\partial p}{\partial x}+\frac{\partial\rho}{\partial y}\frac{\partial p}{\partial y}+\frac{\partial\rho}{\partial z}\frac{\partial p}{\partial z}\right). \tag{5}$$

In Eq. (5), CRHO is another turbulence parameter with a default value equal to 0. In Eq. (3) the diffusion term Diff_T can be expressed as:

$$\begin{aligned}\mathrm{Diff}_T=&\frac{1}{V_F}\left(\frac{\partial}{\partial x}\left(v_kA_x\frac{\partial k_T}{\partial x}\right)+\frac{\partial}{\partial y}\left(v_kA_y\frac{\partial k_T}{\partial y}\right)\right.\\&\left.+\frac{\partial}{\partial z}\left(v_kA_z\frac{\partial k_T}{\partial z}\right)\right),\\v_k=&\mathrm{RMTKE}\left(\frac{\mu}{\rho}\right),\end{aligned} \tag{6}$$

where v_k is the coefficient of turbulent diffusion, which is computed based on the local value of the turbulent viscosity. The turbulent energy diffusion coefficient multiplier RMTKE (with a default value equal to 1.39 for the RNG model and 1 for other models) is a user-defined parameter. In the Prandtl mixing length model, the turbulent kinetic energy k_T affects the dissipation rate. In Flow-3D, the default value of the turbulent mixing length (TLEN) is 7% of the smallest domain dimension. Shojaee Fard and Boyaghchi [17] recommended to select this value equal to 7% of the hydraulic diameter. The default values of TLEN are recommended to provide a value for all turbulence models (except the large eddy model). Rodi [18] stated that the $k-\varepsilon$ model provides reasonable approximations for many types of flows. The turbulent dissipation ε_T should be estimated using an additional transport equation as [16]:

$$\frac{\partial \varepsilon_T}{\partial t}+\frac{1}{V_F}\left(uA_x\frac{\partial \varepsilon_T}{\partial x}+vA_y\frac{\partial \varepsilon_T}{\partial y}+wA_z\frac{\partial \varepsilon_T}{\partial z}\right)$$
$$=C_1\frac{\varepsilon_T}{k}(P_T+C_3G_T)+\mathrm{Diff}_s-C_2\frac{\varepsilon_T^2}{k}, \qquad (7)$$

where C_1, C_2, and C_3 are the user defined coefficients. In the $k-\varepsilon$ model, the default values of these coefficients are $C_1=1.44$, $C_2=1.92$, and $C_3=0.2$. In the RNG model, C_2 is computed based on the turbulent production (P_T) and the turbulent kinetic energy (k_T) terms. The diffusion of dissipation $\mathrm{Diff}_\varepsilon$ is computed as:

$$\mathrm{Diff}_\varepsilon=\frac{1}{V_F}\left(\frac{\partial}{\partial x}\left(v_\varepsilon A_x\frac{\partial \varepsilon_T}{\partial x}\right)+\frac{\partial}{\partial y}\left(v_\varepsilon A_y\frac{\partial \varepsilon_T}{\partial y}\right)\right.$$
$$\left.+\frac{\partial}{\partial z}\left(v_\varepsilon A_z\frac{\partial \varepsilon_T}{\partial z}\right)\right),$$

$$v_\varepsilon=\mathrm{RMDTKE}\left(\frac{\mu}{\rho}\right), \qquad (8)$$

where RMDTKE is the coefficient of turbulent dissipation diffusion. The default values of this parameter for $k-\varepsilon$ and RNG models are 0.77 and 1.39, respectively.

2.3. Numerical methodology

The finite-volume method was used by the CFD package Flow-3D to solve the RANS equations. The computational domain is subdivided into a grid of variable-sized hexahedral cells by Cartesian coordinates. The modeling of free-surface flow over an obstacle using Flow-3D limits the cell conditions within the grid to one of the following conditions: partially solid and fluid, completely solid, partially fluid, completely fluid, and completely empty. Using the Fractional Area/Volume Obstacle Representation (FAVOR) method [19], the spillway is defined as an obstacle in the rectangular domain. The free-surface computation was done using a modified Volume-Of-Fluid (VOF) method [20]. A function of fraction of fluid $F(x,y,z,t)$ is used to reveal the fluid configuration. In a single fluid problem, F reveals the volume fraction occupied by the fluid, where $F=0$, $F=1$, and $0<F<1$ correspond to empty cell, full cells, and partially filled cells, respectively.

3. Description of the model

3.1. Effective parameters

The following equation was used as the head-discharge relationship for a labyrinth spillway [5]:

$$Q=\frac{2}{3}C_dL\sqrt{2g}H_0^{1.5}. \qquad (9)$$

In Eq. (9), Q = discharge, C_d = discharge coefficient, L = total length of labyrinth spillway, g = acceleration due to gravity, and H_0 = total upstream head = $h+V^2/2g$ (V is the approach velocity of flow and h is the approach depth of flow). The numerical models were used to determine Q and H_0 for different geometries of the labyrinth spillways, and C_d data were calculated using Eq. (9). The parameters affecting the discharge of an arced labyrinth spillway can be presented as:

$$Q=f\left(H_0,P,D,L,t',\Theta,w,N,A,\alpha,S_0,g,S_e\right), \qquad (10)$$

where P is the height of spillway; D is the vertical distance from the crest level to the downstream bed level; t' is the thickness of spillway wall; w is the width of a single labyrinth spillway cycle; N is the number of labyrinth spillway cycles; A is the inside apex width; α is the downstream sidewall angle; S_0 is the longitudinal slope of bed; and S_e is the representation of the crest shape (see Figure 1). Using the dimensional analysis and some simplifications, Eq. (10) can be rewritten as:

$$f\left(\frac{Q}{L\sqrt{g}H_0^{1.5}},\frac{H_0}{P},\frac{w}{P},\frac{P}{t'},\frac{D}{P},\frac{A}{t'},N,\Theta,\alpha,S_0,S_e\right)=0. \qquad (11)$$

Since $w/P=2$, $P/t'=8$, $A/t'=1$, $N=5$, $\alpha=6°$, $S_0=0$, and the crest shape was considered the same for all the runs (half-round), these parameters are omitted from Eq. (11). Thus:

$$\frac{Q}{L\sqrt{g}H_0^{1.5}}=f\left(\frac{H_0}{P},\Theta,\frac{D}{P}\right). \qquad (12)$$

From Eqs. (9) and (12) the following is obtained:

$$C_d=f\left(\frac{H_0}{P},\Theta,\frac{D}{P}\right). \qquad (13)$$

The effects of the headwater ratio (H_0/P), the arc angle (Θ), and the relative height ratio (D/P) on the discharge coefficient of labyrinth spillways are presented in the following sections.

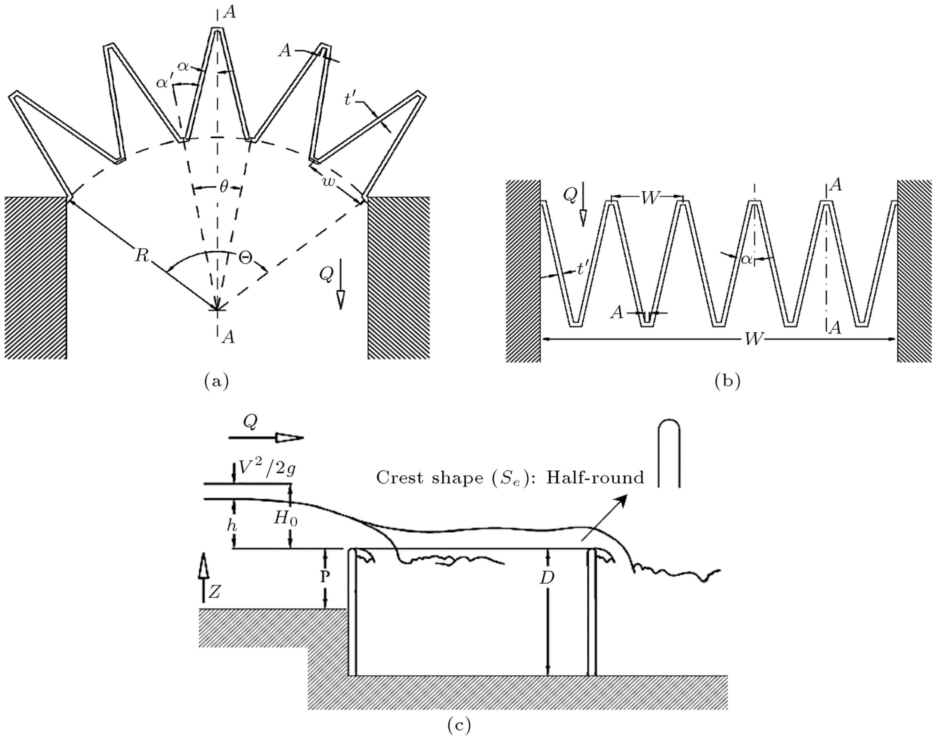

Figure 1. General view of the geometric and hydraulic parameters of labyrinth spillways: (a) Arced configuration; (b) linear configuration; and (c) section A-A view.

3.2. Experimental data

To validate the proposed numerical model, the laboratory data of Crookston and Tullis [11] is used. Crookston and Tullis implemented a physical model of labyrinth spillways in an elevated head box (dimensions: $7.3 \times 6.7 \times 1.5$ m deep) to emulate the conditions of a reservoir. The model characteristics are $\alpha = 6°$, $P = 0.203$ m, $N = 5$, $A = 0.025$ m, $t' = 0.025$ m, $w = 407$ mm, half-round crest shape, and trapezoidal cycles. In addition, data were collected under steady-state conditions without artificial nappe aeration.

3.3. Specification of the numerical model

In this work, the geometry of the labyrinth spillways was defined as an STL (stereo lithography) file using the Catia software, and then was transferred to Flow-3D. As shown in Figure 2, the arced and linear labyrinth spillways were located inside a reservoir and a channel, respectively. The details of the geometries of numerical model are summarized in Table 1.

In the numerical model, the number of computational volumes were increased until the computation time increased disproportionately compared to the achieved accuracy. This was chosen as a criterion and then used for further runs. Flow-3D calculates the time step automatically. The time step was controlled with respect to the criteria of stability and convergence (in the range of 0.0005-0.003 s). The computational domains were extended at least up to a distance of 4P upstream of the spillway crest to avoid the curvature effect of water surface [14,21]. The flow domain is defined as a hexahedral Cartesian coordinates; therefore, the software includes six different boundaries [22]. The upstream boundary condition was introduced as $F = 1$ with a specified water height. The total head and discharge at this section were calculated by Flow-3D

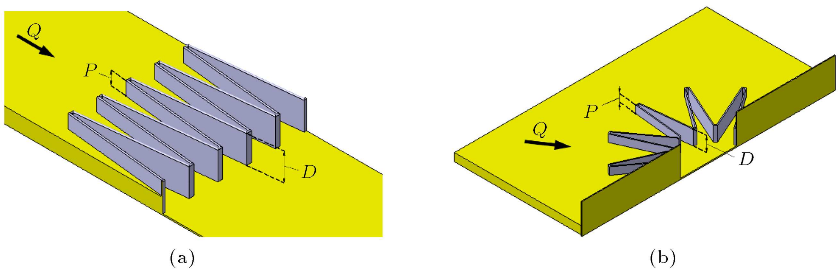

Figure 2. Samples of three dimensional solid of simulated models ($D = 2P$): (a) Linear cycle configuration (in-channel); and (b) arced cycle configuration (in-reservoir).

Table 1. Details of the modeled spillways.

Model no.	α (°)	Θ (°)	L (m)	P (m)	w (m)	t' (m)	A (m)	N	D/P	**Cycle type**	**Crest shape**	H_0/P
1	6	0	15.376	0.203	0.407	0.025	0.025	5	1	Trapezoidal	half-round	0.05 - 0.7
2	6	0	15.376	0.203	0.407	0.025	0.025	5	2	Trapezoidal	half-round	0.05 - 0.7
3	6	150	15.376	0.203	0.407	0.025	0.025	5	1	Trapezoidal	half-round	0.05 - 0.7
4	6	150	15.376	0.203	0.407	0.025	0.025	5	1.5	Trapezoidal	half-round	0.5
5	6	150	15.376	0.203	0.407	0.025	0.025	5	2	Trapezoidal	half-round	0.05 - 0.7
6	6	150	15.376	0.203	0.407	0.025	0.025	5	2.5	Trapezoidal	half-round	0.5
7	6	150	15.376	0.203	0.407	0.025	0.025	5	3	Trapezoidal	half-round	0.5
8	6	150	15.376	0.203	0.407	0.025	0.025	5	4	Trapezoidal	half-round	0.5

Table 2. Meshing and boundary conditions.

Meshing	Number of computational blocks	1-2
	Number of computational volumes	300000-1200000
Boundary conditions	Spillway body	Solid
	Lateral boundaries	Wall
	Inlet	Specific pressure ($F = 1$)
	Outlet	Specific pressure ($F = 0$)
	Between the blocks	Symmetry
Equations	Turbulence model	RNG
	Free surface model	VOF
	Time interval	0.01 s

and were used for further analysis. The meshing and boundary conditions are shown in Table 2. It should be noted that the computational time was between 12 and 72 hours for the models using a personal computer with eight cores of a CPU (Intel E5620 2.4 GHz).

4. Results and discussion

4.1. Numerical model validation

Table 3 shows the numerical simulation error using Flow-3D software. In this table, Q_{measured} represents the measured discharge, $Q_{\text{numerical}}$ represents the simulated discharge, and the error is the percentage difference between the measured and simulated values. This table shows that there is a good agreement between the numerical simulation and experimental results. The maximum difference is 3.2%, which confirms the ability of the numerical simulation to predict the discharge capacity of linear and arced labyrinth spillway.

Table 3. A comparison between the numerical and experimental values of head-discharge.

Model no.	H_0/P	Q_{measured} (m^3/s)	$Q_{\text{numerical}}$ (m^3/s)	**Error (%)**
1	0.2	0.178	0.182	2
	0.3	0.259	0.263	1.8
	0.7	0.535	0.547	2.4
3	0.05	0.030	0.031	2.7
	0.1	0.093	0.095	1.9
	0.3	0.272	0.278	2.2
	0.5	0.360	0.372	3.2
	0.7	0.433	0.446	3

4.2. Effects of hydraulic head

Figure 3 shows the variations of the discharge coefficient of the linear and arced labyrinth spillways with respect to H_0/P when $\alpha = 6°$ and $D/P = 1$ and 2. The results show that in the low head

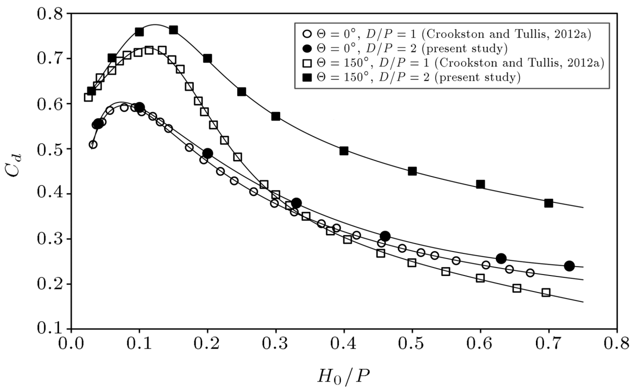

Figure 3. Discharge coefficient variations with H_o/P for different values of Θ and D/P.

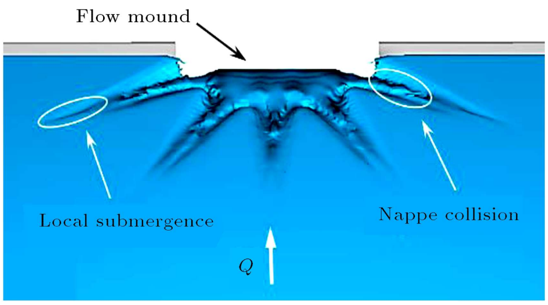

Figure 4. Flow feathers due to the convergence of flow passing over an labyrinth spillway ($H_0/P = 0.3$, $\Theta = 150°$, and $D/P = 1$).

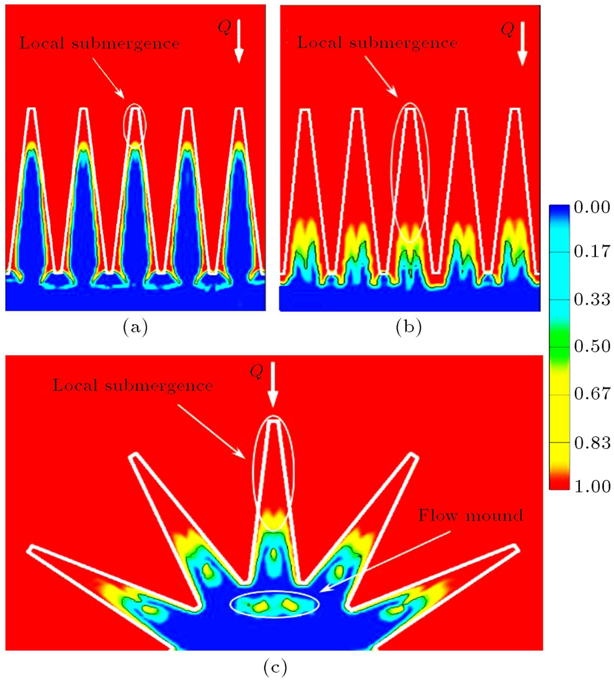

Figure 5. Contours of fraction of fluid (F) at the crest elevation of the labyrinth spillways ($D/P = 1$): (a) $\Theta = 0°$ at $H_0/P = 0.3$; (b) $\Theta = 0°$ at $H_0/P = 0.7$; and (c) $\Theta = 150°$ at $H_0/P = 0.3$.

conditions, a labyrinth spillway behaves similar to a linear spillway ($\alpha = 90°$), so that C_d is an increasing function of H_0/P [23]. However, by increasing H_0/P, C_d reaches to a maximum value, then it becomes a monotonic decreasing function of H_0/P. To justify the decreasing trend of the discharge coefficient of the labyrinth spillways, it should be noted that in the vicinity of the upstream apexes, due to the interaction of the flow over adjacent sidewalls (thereafter called nappe interference), the discharge over the spillway decreases. Depending on the labyrinth spillway geometry and the flow conditions, the nappe interference region may include a nappe collision region, a local submergence region, or both (see Figure 4). At lower values of H_0/P, nappe interference includes only a nappe collision region. However, at higher values of H_0/P, if the labyrinth spillway flow becomes larger than the outlet cycles free-flow capacity, the portion of adjacent to the upstream apex becomes submerged [11]. As a result, the discharge capacity decreases.

Figure 5 represents a typical fraction of fluid contours at the crest elevation of the spillway ($z = 0.203$ m). According to this figure, an increase in the headwater ratio leads to an increase in the size of the local submergence region. Therefore, at higher values of H_0/P, the labyrinth spillway may be entirely submerged. Overally, it can be concluded that an increase in the headwater ratio increases the nappe interference and hence the size of the local submergence region. As a result, decreasing trend of C_d occurs. For the trend lines fitted to the data of Figure 3, the following equation is derived to represent the discharge coefficient:

$$C_d = \frac{A_1\left(\frac{H_0}{P}\right)^3 + A_2\left(\frac{H_0}{P}\right)^2 + A_3\left(\frac{H_0}{P}\right) + A_4}{\left(\frac{H_0}{P}\right)^2 + A_5\left(\frac{H_0}{P}\right) + A_6}, \qquad (14)$$

where A_1 to A_6 are the equation coefficients. By using the least squares method, the values of coefficients were obtained as shown in Table 4. The correlation coefficients (R^2), due to Eq. (14), are also indicated in this table. The values of R^2 confirm that there is a good agreement between the proposed equation and the data presented in Figure 3. Eq. (14) is valid for the range of $0.05 \leq H_0/P \leq 0.7$.

4.3. Effects of arc angle

As shown in Figure 3, the arced configuration in the low head conditions can increase the hydraulic efficiency of the labyrinth spillway. Figure 6 shows the approach flow velocity field for an arced labyrinth spillway when $H_0/P = 0.3$ and 0.6. According to this figure, the hydraulic efficiency increment of the arced labyrinth spillway is caused by the improvement in the alignment of the cycles with respect to the approach

Table 4. Trend line coefficients for labyrinth spillways.

Model no.	A_1	A_2	A_3	A_4	A_5	A_6	R^2
1	-0.0146	0.08413	0.11181	0.00356	0.05353	0.01118	0.998
2	0.34998	-0.40385	0.38426	-0.00253	0.40078	0.00438	0.999
3	-0.27036	0.41802	-0.0975	0.01803	-0.24191	0.03108	0.998
5	-0.18372	0.49636	-0.0667	0.01383	-0.18521	0.02416	0.997

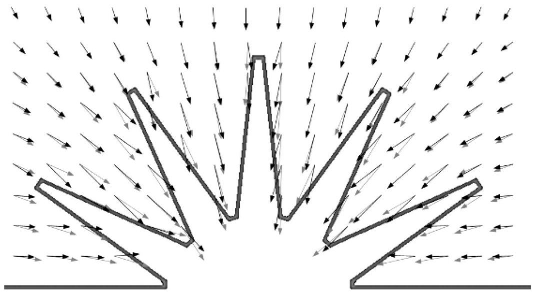

Figure 6. Approach flow velocity vectors at 0.6th depth of flow for an arced labyrinth spillway ($\Theta = 150°$, $D/P = 1$, $H_0/P = 0.3$ (black), and $H_0/P = 0.6$ (grey)).

flow. However, the orientation of the velocity vectors change with H_0/P and deviate more from the ideal condition (perpendicular to the crest) by increasing this parameter. These results well match with those reported by Christensen [15].

Figure 3 also shows that for $D/P = 1$, the trend of variations of the discharge coefficient with H_0/P is more for the arced labyrinth spillway in such a way that in higher head conditions, the discharge coefficient of the arced labyrinth spillway is smaller than that of a linear labyrinth spillway. The reason is that for a specific α, α' increases when Θ increases. As a result, a larger inlet cycle flow area occurs. Therefore, compared to a linear labyrinth spillway, an arced labyrinth spillway spills more flow into the downstream cycles and leads the larger local submergence area for a given head (see Figure 5). In addition, in an arced labyrinth spillway, the convergence of the flow exiting the labyrinth cycles forms a mound in the downstream channel, which may act as an obstacle against the spilling flow (see Figures 4 and 5(c)).

4.4. Effects of the downstream bed level

According to the results presented in previous sections, the local submergence condition has a significant role on the discharge coefficient of the labyrinth spillways. For increasing the discharge capacity of the outlet cycles, the downstream bed level is lowered. According to Figure 3, the discharge coefficient of the labyrinth

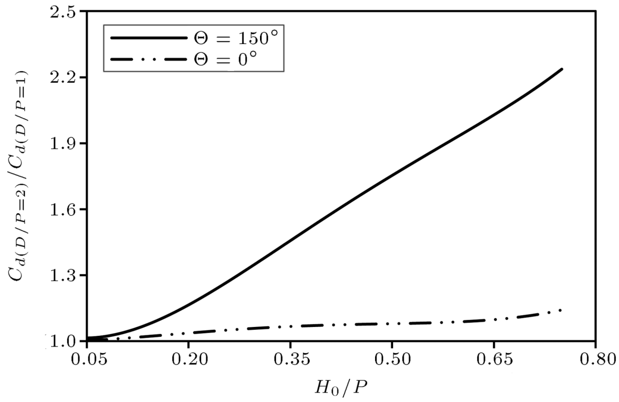

Figure 8. Improvement of the hydraulic performance of labyrinth spillways by lowering the downstream bed level.

spillways increases when D/P increases. This may be due to the reductions of the local submergence region area and the mound height (see Figure 7).

Figure 8 shows the variation of the ratio of the discharge coefficient of the linear and arced labyrinth spillways for $D/P = 2$ to the discharge coefficient for $D/P = 1$. It can be observed that the hydraulic benefits of lowering the downstream bed level are more significant for higher values of H_0/P and Θ. By increasing these two parameters, the area of local submergence region and its negative effect on the hydraulic performance of the labyrinth spillway increases (see Figure 5). Therefore, the advantages gained from the increase in D/P are more remarkable in these circumstances. For example at $H_0/P = 0.7$, the discharge coefficient of the arced labyrinth spillway with $D/P = 2$ is about twice as compared to $D/P = 1$. Figure 9 shows a typical variations of the discharge coefficient for an arced labyrinth spillway with respect to D/P when $H_0/P = 0.5$ and $\Theta = 150°$. Based on Figure 9, the discharge coefficient of the arced labyrinth spillway increases with an increase in D/P. It, then, remains almost constant for higher values of D/P. Figure 9 also indicates that for the mentioned conditions, the discharge coefficient of the arced labyrinth spillway

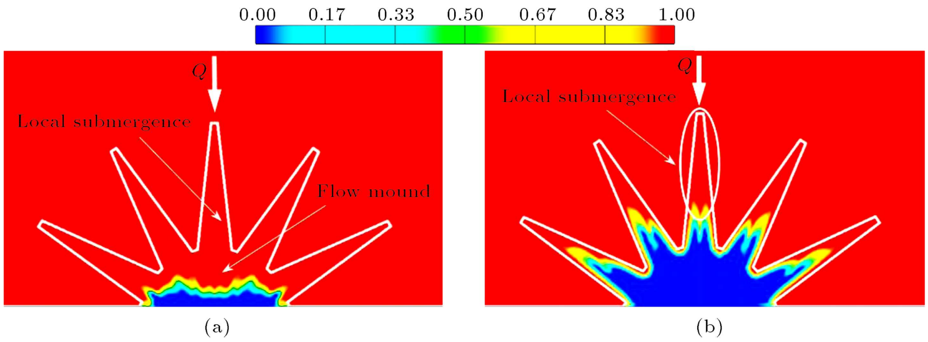

Figure 7. Contours of fraction of fluid (F) at the crest elevation of the labyrinth spillway ($H_0/P = 0.7$, $\Theta = 150°$): (a) $D/P = 1$; and (b) $D/P = 2$.

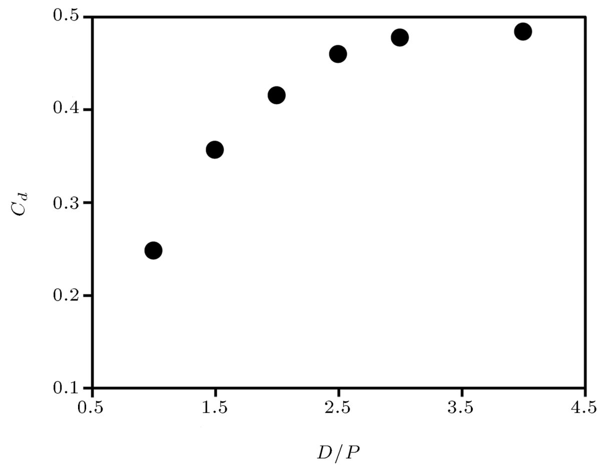

Figure 9. C_d versus D/P for the arced labyrinth spillway ($H_0/P = 0.5$, $\Theta = 150°$).

increases up to about 100% by increasing D/P. However, the downstream bed level does not propose a significant effect when D/P exceeds 3, because, the local submergence is not large enough to influence the discharge coefficient. It should be noted that although lowering the downstream bed level eliminates local submergence, it does not eliminate the nappe interference.

5. Conclusions

This paper studies the hydraulic performance of the labyrinth spillways using the Flow-3D software. Comparison between the presented numerical simulations with previously reported experimental results validates the ability of Flow-3D to simulate the flow over labyrinth spillways with an acceptable accuracy. The simulation results show that nappe interference and local submergence have important roles in the spillway performance. In the low head conditions, the discharge coefficient of a labyrinth spillway is an increasing function of H_0/P. However, C_d reaches to a maximum value and, then, becomes a monotonic decreasing function of H_0/P. The comparison between the discharge coefficients of the arced and linear labyrinth spillways shows that this coefficient is greater for the arced spillway in the low head conditions. However, in the high head conditions, the opposite behavior is observed due to the formation of local submergence region and flow mound. Also, the downstream bed level has an important role on the performance of the labyrinth spillways. By lowering the downstream bed level, the discharge coefficient increases, especially for arced labyrinth spillways. This behavior continues until the discharge coefficient reaches to a constant value. The mentioned approach can be used to decrease the effect of local submergence on the performance of labyrinth spillways.

Acknowledgments

The authors would like to express their appreciation to the Applied Research Office of the Iran Water Resources Management Company (IWRMC) for financially supporting this study through project RIV4-91042. They also thank Mr. Younes Sangsefidi (graduate research assistant at EECS department, Washington State University, WA, USA) for his help in editing the manuscript.

References

1. Hay, N. and Taylor, G. "Performance and design of labyrinth spillways", *J. Hydraul. Div.*, **96**(11), pp. 2337-2357 (1970).
2. Darvas, L.A. "Discussion of 'Performance and design of labyrinth spillways,' by Hay and Taylor", *J. Hydraul. Eng., ASCE*, **97**(80), pp. 1246-1251 (1971).
3. Lux, F. and Hinchliff, D.L. "Design and construction of labyrinth spillways", *15th ICOLD Congress*, **IV**, Q59-R15, Lausanne, Switzerland, pp. 249-274 (1985).
4. Megalhaes, A.P. and Lorena, M. "Hydraulic design of labyrinth spillways", Report No. 736, National Laboratory of Civil Engineering, Lisbon, Portugal (1989).
5. Tullis, J.P., Amanian, N. and Waldron, D. "Design of labyrinth spillway spillways", *J. Hydraul. Eng.*, **121**(3), pp. 247-255 (1995).
6. Khode, B.V., Tembhurkar, A.R., Porey, P.D. and Ingle, R.N. "Experimental studies on flow over labyrinth spillway", *J. Irr. Drainage Eng.*, **138**(6), pp. 548-552 (2012).
7. Falvey, H.T. "Hydraulic design of labyrinth spillways", *ASCE*, Reston, VA (2003).
8. Tullis, B.P., Young, J. and Chandler, M. "Head-discharge relationships for submerged labyrinth spillways", *J. Hydraul. Eng.*, **133**(3), pp. 248-254 (2007).
9. Ghodsian, M. "Stage-discharge relationship for a triangular labyrinth spillway", *Proc. Inst. Civ. Engrs., Water Management*, **162**(3), pp. 173-178 (2009).
10. Carollo, G.F., Ferro, V. and Pampalone, V. "Experimental investigation of the outflow process over a triangular labyrinth spillway", *J. Irr. Drainage Eng.*, **138**(1), pp. 73-79 (2012).
11. Crookston, B.M. and Tullis, B.P. "Arced labyrinth weirs", *J. Hydraul. Eng.*, **138**(6), pp. 555-562 (2012).
12. Crookston, B.M. and Tullis, B.P. "Discharge efficiency of reservoir-application-specific labyrinth weirs", *J. Hydraul. Eng.*, **138**(6), pp. 564-568 (2012).
13. Kumar, S., Ahmad, Z., Mansoor, T. and Himanshu, S.K. "Discharge characteristics of sharp crested spillway of curved plan-form", *Research J. of Eng. Sciences*, **1**(4), pp. 16-20 (2012).

14. Kumar, S., Ahmad, Z., Mansoor, T. and Himanshu, S.K. "A new approach analyze the flow over sharp crested curved plan form spillways", *Intl. J. Recent Technology and Eng.*, **2**(1), pp. 24-28 (2013).
15. Christensen, N.A. "Flow characteristics of arced labyrinth weirs", M.S. Thesis, Utah State University, Logan, Utah (2013).
16. Flow-3D, *User Manual Version 9.3*, Flow Science, Inc., Santa Fe (2008).
17. Shojaee Fard, M.H. and Boyaghchi, F.A. "Studies of the influence of various blade outlet angles in a centrifugal pump when handling viscous fluids", *American J. of Applied Sciences*, **4**(9), pp. 718-724 (2007).
18. Rodi, W. "Turbulence models and their application in hydraulics", *IAHR Monograph*, Delft (1980).
19. Hirt, C.W. and Sicilian, J.M. "A porosity technique for the definition of obstacles in rectangular cell meshes", *Proc. 4th Intl. Conf. Numerical Ship Hydrodynamics*, National Academy of Science, Washington, DC, September, pp. 1-19 (1985).
20. Hirt, C.W. and Nichols, B.D. "Volume of fluid (VOF) method for the dynamics of free boundaries", *J. of Comput. Phys.*, **39**, pp. 201-225 (1981).
21. Anderson, R.M. and Tullis, B.P. "Comparison of piano key and rectangular labyrinth weir hydraulics", *J. Hydraul. Eng.*, **138**(4), pp. 358-361 (2012).
22. Kermani, E. and Barani, G.A. "Numerical simulation of flow over spillway based on the CFD method",*Scientia Iranica, Trans. A*, **21**(1). pp. 91-97 (2014).
23. Swamee, K.P. "Generalized rectangular weir equation", *J. Hydraul. Eng.*, **114**(8), pp. 945-949 (1988).

Biographies

Yousef Sangsefidi received his MSc degree in Hydraulic Structures from Tarbiat Modares University (TMU), Tehran, Iran, in 2014. He is currently a PhD Student at Tarbiat Modares University. His research interests include flow control structures, flow and sediment transport in rivers, energy dissipation structures, and response surface methodology.

Mojtaba Mehraein received PhD degree in 2011, from Tarbiat Modares University. His research interests include experimental and numerical investigation of scour and flow field around the hydraulic structures. He is currently Assistant Professor at Kharazmi University of Tehran.

Masoud Ghodsian obtained his PhD in 1992 from Indian Institute of Technology-Roorkee, India. He started his academic and research activities when he joined Tarbiat Modares University, Tehran, Iran, in 1992. He has published about 80 peer reviewed journal papers and about 160 papers in international and national conferences. His field of research activities includes: river engineering, hydraulic structure, scouring and sediment transport.